Chapter 2
Experimental Methods for Aerodynamics

Richard Green

Abstract Experimental techniques for aerodynamics have been essential tools for the development of rotorcraft. This includes wind tunnel, water tank testing, and flight testing. Rotor flows are rich in their physical complexity, and consequently an awareness of range of experimental methods is required. The chapter contains an introduction to wind tunnels, followed by a description of important experimental techniques, such as flow visualisation, pressure measurements, force and moment measurements, thermal anemometry and instrument calibration. Their performance and relative merits are discussed. Results are presented include forces and moments on a rotor, dynamic stall, particle-image velocimetry of a vortex ring state, and more.

Nomenclature

BOS	Background-Oriented Schlieren
CTA	Constant Temperature Anemometry
LDA	Laser Doppler Anemometry
PIV	Particle Image Velocimetry
POD	Proper Orthogonal Decomposition
VRS	Vortex Ring State
A_p	particle displaced fluid inertia force
B	particle Basset history force
C	tracer particle parameter
C_p	pressure coefficient
c	chord length; speed of light for Doppler effect
D	notional wind tunnel dimension; drag force
D_p	particle viscous drag force
d_p	particle diameter
$\underline{e}_b$	incident beam direction vector from laser

Supplementary Information The online version contains supplementary material available at https://doi.org/10.1007/978-3-031-12437-2_2.

R. Green (✉)
School of Engineering, University of Glasgow, Glasgow, Scotland
e-mail: richard.green@glasgow.ac.uk

A. Filippone and G. Barakos (eds.), *Lecture Notes in Rotorcraft Engineering*,
Springer Aerospace Technology, https://doi.org/10.1007/978-3-031-12437-2_2

$\underline{e}_{pr}$	Doppler shifted scattered light direction vector, particle to receiver
f	frequency
f_b	incident laser beam frequency
f_D	frequency shift due to Doppler effect; difference in Doppler shifts for dual beam
f_r	Doppler shifted light frequency perceived at receiver
N_s	particle Stokes number, $\sqrt{\nu_f/\omega d_p^2}$
p	fluid pressure
P	force on particle due to flow field pressure gradient
R	rotor radius
r	radial ordinate
t	time
U	flow velocity
U_∞	wind tunnel free stream velocity
(u, v, w)	fluid flow velocity components in Cartesian reference
u_f	fluid velocity
$\underline{u}_p$	tracer particle velocity vector
u_p	tracer particle velocity
u_{pr}	particle radial velocity
u_θ	fluid velocity in tangential direction
V	relative velocity, flow speed ; hot-wire voltage
$\underline{V}$	fluid or particle velocity vector
(x, y, z)	spatial ordinates in Cartesian sense

Greek Symbols

α	aerodynamic angle of attack
α	particle motion phase relative to fluid
α	receiver axis direction for Doppler effect analysis
β	aerodynamic sideslip angle; velocity direction for Doppler effect analysis
Δs	particle displacement
$\Delta \underline{s}$	particle displacement vector
Δt	time difference, PIV time delay
η	particle to fluid velocity amplitude ratio
θ	angle between incident beams
λ	light frequency
ν_f	fluid kinematic viscosity
ρ_f	fluid density
ρ_p	particle density
σ	ratio of particle to fluid density
ξ	parametric ordinate
ω	circular frequency, angular velocity

2.1 Introduction

The flow around a rotorcraft in even its simplest mode of flight is extraordinarily complex. It comprises entanglements of multiple trailed vortex systems, regions where compressibility effects are significant, areas of separated flow, and the flow can be regarded as unsteady and subject to significant interaction effects. A successful experimental test campaign may have to isolate specific phenomena, or investigate performance aspects of the flight vehicle, but the complexity of the flow is always a challenge. Crucially, if the aeromechanics of the flight vehicle have to be represented, then test models can be very challenging to design. While issues with fixed wing wind tunnel testing might be limited by available test Reynolds and Mach numbers, testing for rotorcraft needs to consider additional parameters such as advance ratio, trim condition.

A good skill-set is required for a researcher to be able to conduct an experiment successfully. Not only is a thorough knowledge of fluid mechanics and aerodynamics a pre-requisite, but a solid appreciation of wider aspects of physics, optics, electronics are essential. For aircraft and related testing, the wind tunnel practitioner needs a wider appreciation of aeronautics, interest in aerodynamics is not sufficient of its own. Expertise with mathematics and statistics are expected, and computing systems for instrumentation and data analysis are tools of the trade. A wind tunnel control room in the middle of a test campaign should be a calm place, there is much planning and coordination required to bring a test programme to life, but plenty can go wrong, and the ability to think on one's feet, problem solve in the moment, get one's hands dirty are the types of activity to expect. The theoretician or CFD specialist without prior experience in experimental testing is encouraged to work on an experimental programme; the reader is referred to Ref. [1] for a wider understanding of theory and practice.

The reader is expected to have a clear idea of why an experimental test campaign should be done, but may not have any *a priori* familiarity with experimental testing. *All* experimental work requires extensive planning. Inexperience and excessive eagerness to get started are a bad combination that leads to much wasted time and resource. In this respect the chapter is an overview. It takes the reader through basic wind tunnel layout and operating limitations, provides a background to the most essential techniques that the reader needs to gain an awareness of, and finishes with an introduction to the more sophisticated optical flow field measurement methods. The experimentalist should not attempt these more advanced methods without first considering the capabilities of the apparently less sophisticated techniques, and a particular emphasis is placed upon the importance of doing force and moment measurement and on the researcher being productive.

The reader is encouraged to gain a thorough understanding of wind tunnels and test techniques before any experimental design and testing is attempted, and regular reference is made to some important reference publications.

As a final comment to this introduction, wind tunnels can be expensive to build and use. Operating economics are a concern. Their demise due to the development of CFD has been predicted for a long time, but recent initiatives such as the UK National Wind Tunnel Facility have recognised their strategic value as a research base.

2.2 The Wind Tunnel

There are facilities other than wind tunnels available for experimental aerodynamics (towing tanks, whirl tower, testing chamber, flight testing), but the wind tunnel is the most commonly used instrument. We restrict the discussion to low-speed tunnels, as this is appropriate for the flight regime of rotorcraft. The reader is referred to the text by Barlow, Rae and Pope [2] for a broad overview of low-speed wind tunnel testing.

The wind tunnel generates a conditioned flow at free stream speed U_∞ in a carefully controlled and monitored environment. Experiments are usually conducted in the working section, which are generally *closed jet* section or an *open jet section*. Figure 2.1 shows images of test models in an open section and closed section jet respectively. The open jet arrangement has no confining walls and has the advantage that the flow streamtube around the model is not so strictly confined as with the closed section. Access to the test model is relatively unrestricted, but the lack of a floor can lead to safety issues.

The flow may circulate around a loop (return), for which the advantage is lower running cost, or in the case of a non-return tunnel the flow is exhausted out into the atmosphere downstream of the test section. Thus, a wind tunnel may be described as closed-return, for example. The closed-return tunnel is a commonly found type,

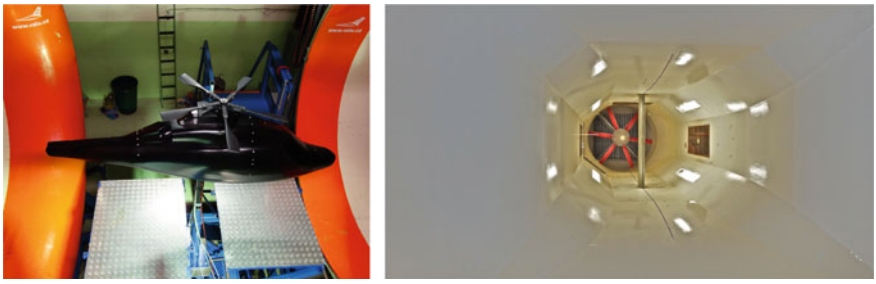

Fig. 2.1 Wind tunnel working sections. **a** helicopter wind tunnel model (quarter scale Dauphin) in open-jet wind tunnel (VZLU, Prague, CZ); **b** 2-D dynamic stall model in closed section wind tunnel (HP tunnel, University of Glasgow, UK)

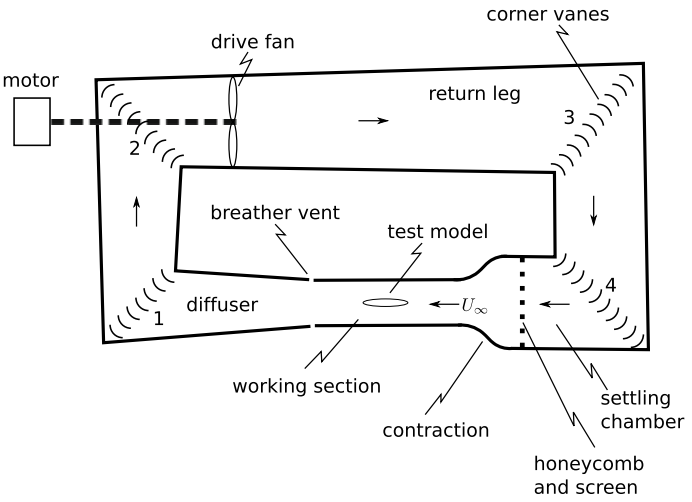

Fig. 2.2 Schematic diagram of a closed-return wind tunnel

and Fig. 2.2 shows a schematic diagram of a typical example. The flow direction in this diagram is clockwise.

The working section with test model are indicated. Atmospheric tunnels have breather vents at the end of the working section. Flow leaving the working section passes into a diverging diffuser and then encounters the first set of corner vanes. These turn the flow efficiently by 90° to a continued leg of the diffuser and another set of corner vanes 2. The flow then passes through the drive fan that raises the stagnation pressure of the flow. The return leg continues the diffusing section, there is corner vanes set 3, additional diffusion followed by corner vanes 4. The flow then passes into the settling chamber at its minimum speed, the function of the settling chamber is to give time for disturbances in the flow to settle and dampen out. Flow straightener and a screen are often fitted inside the settling chamber, which help to remove swirling motion and turbulence from the flow. The flow then passes through the contraction, where it is accelerated to the test section velocity U_∞. A general rule is that flow quality in the working section expressed in terms of turbulence level is improved with a higher ratio of contraction entry area to working section entry area (the contraction ratio). The disadvantage is a much larger wind tunnel size for a given working section size.

Wind tunnel operation costs are extremely important. The ideal wind tunnel is one that is as large as possible and runs at any desired speed. Very large wind tunnels occupy an enormous amount of space, power requirements increase as a function of the square of the size and the cube of the speed. Forces and moments on wind tunnel test models need consideration; achieving a very small increase of Reynolds number might be at the expense of a huge increase of dynamic pressure and model size, the model needs to be strong enough. A compromise has to be reached, and it is a case of understanding what type and size of wind tunnel is suited for a given task.

Table 2.1 Relative merits of instrumentation systems other than scientific benefits

Instrumentation	Cost	Complexity	Training	Calibration	Maintenance	Safety risk	Difficulty
Model positioning	VH	H	Some	Infrequent	Yes	H	L
Force/moment balance	M/VH	M	Some	Infrequent	No	L	L
Flow visualisation	L/M	M/H	Some	No	Little	M/H	M/H
Pressure probes	L/M	M	No	Infrequent	No	L	M
Pressure scanners	L/M	H	No	Generally no	No	L	M
CTA	M	H	Yes	Always	Wire repair	L	H
LDA	VH	VH	Yes	No	Yes	VH	VH
PIV	VH	VH	Yes	Always	Yes	VH	VH

L low, *M* moderate, *H* high, *VH* very high

2.3 Benefits of Wind Tunnel Instrumentation Types

A measurement technique should be used because of the scientific or engineering value of the data it provides. Instrumentation is costly, and some items are expensive to maintain and, in fact, difficult to live with. Furthermore, the user must bear in mind likely costs in the event of equipment failure. Skilful use of an inexpensive technique is a better achievement than poor use of one that relies on highly sophisticated instrumentation. This is important for the uninitiated, where the opportunity to learn is of paramount importance, and Table 2.1 is intended to give some idea of the pros and cons of some of the most widely available methods. As an example, the inconvenience of wire repair for the Constant Temperature Anemometry (CTA) technique is often cited as a reason to not use the hot-wire technique, but the wires themselves are often only broken during handling. The solution is a stock of replacements, and, ideally, a repair kit. Contrast this with the repair or replacement costs of a major system component for PIV, never mind the difficulties of working with class 4 lasers. Calibration for CTA is also cited as an inconvenience, but a calibration process for PIV must be also done, and neglect of the state of the elements of a PIV system that affect the calibration will result in an unknown drift and error. Calibration of instruments where it is necessary is an essential step in guaranteeing the quality of data, and should never be viewed as a hindrance.

2.4 Force and Moment Measurements

Wind tunnel test models need to be mounted in wind tunnels. This provides an obvious way of measuring the aerodynamic forces and moments, as the measurement system can be integrated with the model mounting and positioning system. *Most* wind tunnel testing is for force and moment measurement, this simple matter of fact can be quite

easily forgotten. *Most* flow field investigation is only of interest because there is some effect on an aerodynamic force or moment to be investigated. The wind tunnel model shown in Fig. 2.1a is mounted on a stiff strut, which can be seen emerging below the belly of the model. The model fuselage is in turn attached to a six component force balance inside the model mounted at the end of the strut. The wind tunnel model shown has a separate loads measurement system for the stub rotor, allowing the hub drag to be separated from the fuselage drag. The wind tunnel model in Fig. 2.1b is instrumented with surface mounted pressure transducers (see later section), and pressure may be integrated to provide some information about the aerodynamic loading.

2.4.1 Model Positioning System and Balance Systems

The model must be positioned in the wind tunnel, and its attitude and orientation should be varied with ease. The simplest model positioning system should allow for variation of angle of attack, and more sophisticated turntable systems allow for variation of model yaw, pitch and roll angle. The flight dynamics requires aerodynamic data to be expressed in a particular way, and the aerodynamicist can frequently be ignorant of the sign conventions and flow directions that flight dynamicists use. Model attitude in terms of yaw, pitch, roll, for example, will need to be expressed in terms of angle of attack α and sideslip β.

Force measurement can be performed with something as simple as a single component load cell, but whatever device is used the researcher must be familiar with its design and theory of operation. Balances can be extremely delicate, but all balances are vulnerable to being mishandled. The model mounting position relative to the moment resolution centre of the balance must be known if sense is to be made of measured moments

External Force Balance. This type of balance is outside the wind tunnel; a photograph of such a balance is indicated in Fig. 2.3a. The model is mounted onto the balance by struts, and it allows for some yaw and roll angle adjustment in addition to pitch. The balance design is very stiff indeed, and the whole system benefits from high inertia in addition to the stiffness. This balance design produces particularly accurate forces and moments, and calibration can take place in-situ.

Sting Balance. This type of mounting and balance system offers the flexibility of high yaw, pitch and roll angles at the expense of mounting stiffness and smaller inertia. Ideally the sting and balance are inside the model, and this can make for a complex model installation procedure. A diagram of a sting-balance system is shown in Fig. 2.3b. A typical balance is shown in Fig. 2.4a, the flexural elements and strain gauges can be seen. The ground end fits to the sting, the model is mounted on the live end.

Rotating Shaft Balance. These are balances purpose built for mounting on rotating shafts. They can be used for propeller and rotor forces, for example for individual

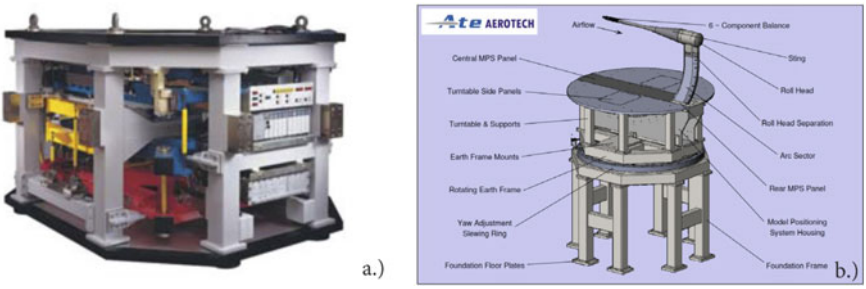

Fig. 2.3 External **a** and internal **b** wind tunnel balance systems. The external balance sits entirely underneath or over the working section, and the model is mounted to the balance via struts. (ATE Aerotech, UK)

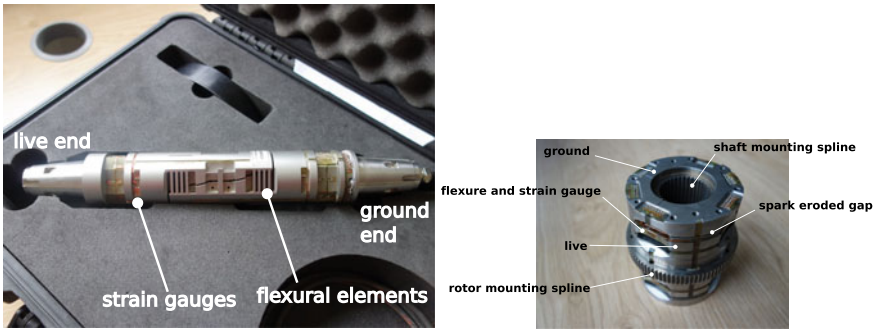

Fig. 2.4 Some six component balances. To the left, sting balance (ATE Aerotech, UK); to the right, rotating shaft balance (Aircraft Research Association, UK)

blade forces and moments. A rotating shaft balance is shown in Fig. 2.4b. It is manufactured from two concentric elements with an annular gap, the inner part is the ground side, connected to the rotor shaft, the outer part is the live side, connected to the rotor assembly. Flexural elements are manufactured that bridge the ground and live sides, and gaps between the live and ground side elsewhere are manufactured using a technique such as spark erosion. Excitation voltage signals to the strain gauges and strain gauge signals fed across are slip rings or via a telemetry system.

2.4.2 Balance Calibration

Balances have to be manufactured with great care, and handled in such a way. Careful balance calibration is essential, and this procedure must be documented. Specialised jigs are required, and calibration must take place in a carefully controlled environment. The calibration process only guarantees the best accuracy of the balance

system. In use the model position will deform and balance signals drift, the user must be aware of this and factor these effects in when stating accuracy of the actual measurement.

2.5 Flow Visualisation

A flow visualisation test is regarded as an essential component of any test campaign. In some cases it may be completely impractical to do, but where it is possible, it should be attempted. Most flow visualisation methods are low cost, and a consumer camera is often all that is needed for image recording. Specialist or high-end cameras are only required where a particular performance demands it. Illumination methods include flood lights, UV lights, strobe lights and continuous or pulsed lasers. Safety precautions are often necessary; in the cases of use of lasers and stroboscopes this is obvious, but use of oil may create slip hazards. The flow visualisation method works by making some property of the flow visible, this may be to visualise the flow over the body surface, or to see features of the developing flow field. A flow field visualisation is recommended in advance of any test involving PIV. Some flow visualisation methods are as follows.

Surface Tufts. This is a useful technique for visualisation of attached or separated, steady or unsteady flows over a body. The tufts align with the local flow direction adjacent to the surface. Tufts are typically short pieces of thin thread stuck to the model surface with glue or tape. The tuft colour should be in good contrast with the surface, and fluorescent tufts illuminated with UV light create a very strong contrast, but normal lighting is the usual technique. A stills or video camera is sufficient for recording the tuft alignment. High speed video photography with appropriate image post-processing can show the fluctuation of the tuft position, useful for the interpretation of unsteady, separated flow.

China Clay. A mixture of china clay and paraffin is poured onto the model surface. The mixture must be runny enough for the flow to move the mixture, but thick enough so that it does not flow over vertical surfaces too easily. When the wind tunnel is turned on the wall shear stress moves the china clay mixture over the model surface, and the paraffin dries off. Surface streamlines and separation lines are revealed. It will show a time mean effect, and the mixture will tend to settle and remain wet in quiescent zones where surface shear is very low. China clay visualisation can create some beautiful images, and different coloured dye in the china clay can be used to indicate where specific areas of flow track to. It is useful for streamlined bodies, and is excellent for revealing the effects of excrescences and details at body junctions. The dried mixture is cleaned off easily after a test. Note that tape must be applied over any pressure tappings on the model, otherwise the tappings will be blocked.

Smoke Flow. Smoke flow patterns reveal details of the flow field; the user must be aware of the difference between a streakline, a streamline, and a particle path

line. Smoke flow visualisation works best when the smoke plume is dense, flow field turbulence can mix the smoke plume reducing contrast. The injection point of the smoke into the flow is critical, it has to be entrained into the desired region of flow. Smoke plumes are typically created using a wand with a heated tip, oil is pumped onto the tip of the wand where it vapourises to form the distinct smoke. Moving the smoke wand around will show how the flow deviates over the various parts of a test body. Smoke flow can be used to visualise inflows, wakes, vortices, and can trace out separated zones. It is particularly useful for the visualisation of unsteady flows.

Schlieren and Shadowgraph. These techniques are usually associated with visualisation of transonic and supersonic flows, but they have been used to great effect for visualisation of flows around rotors and entire helicopters. Change of air density causes a change of refractive index, thus changing the path of a light ray. The Schlieren method reveals the spatial density gradient, shadowgraph the second derivative. The article by Bagai and Leishman [3] provides an analysis of Schlieren and shadowgraph methods for rotor flows, and the reader is encouraged to consult this article as a useful starting point. Ref. [4] shows an interesting application of the shadowgraph method. Recently, the technique of Background Oriented Schlieren (BOS) has been used to great effect. In this technique an image of a background pattern is compared with the image of the background pattern behind the flow field. The image processing required is lengthy, but the technique can be used in the laboratory and in flight testing, see the articles by Raffel [5] and Kindler et al. [6]. In particular, BOS has the advantage that some quite straightforward instrumentation is the only requirement.

2.6 Pressure Measurement

Pressure measurement in fluid mechanics is a particularly powerful technique. It is almost always used for determining the flow speed in the wind tunnel, and pressure can be measured to infer flow speed elsewhere or to determine surface flow features and be integrated to provide loads and moment information. Pressures measured on the wind tunnel wall surfaces can be used to calculate body lift, pressure measured in a body wake will provide drag, and these techniques can lead to low cost of model production. Pressure sensors tend to be in the form of pressure scanners or individual pressure transducers, and high performance pressure transducers have frequency responses up to several tens of kHz, so may be used for unsteady aerodynamics, measurement of turbulence phenomena, aeroacoustics. Pressure measurement by arrays of probes can provide all three velocity components at a point and even vorticity. An appreciation of pressure measurement is therefore a pre-requisite for any experimentalist.

Pitot-Static Probe. This type of pressure probe measure the flow stagnation pressure at the probe tip, and the probe static pressure at a location some distance behind the tip. The difference between these two pressures is the local dynamic pressure. How

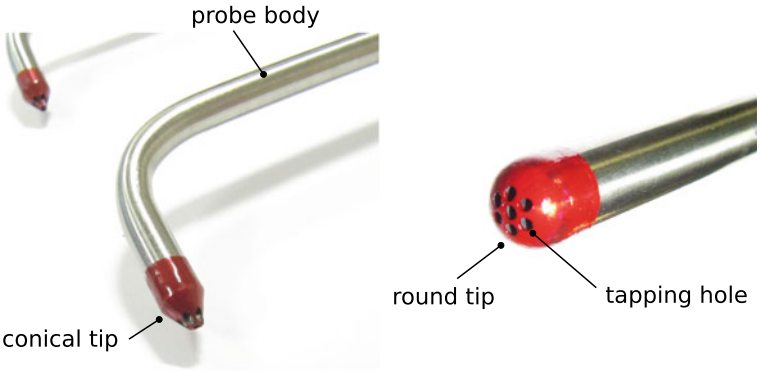

Fig. 2.5 Multi-hole probes for flow field pressure and velocity measurement (Surrey Sensors Ltd, UK)

the probe is used depends upon the application, but they are typically used to obtain wind tunnel free stream speed, and arrays of these probes are used for wake and jet surveys.

Multi-hole Probe. The basic Pitot-static probe cannot measure flow direction. Multi-hole probes consist of a specially profiled probe tip with a tapping hole at the front and an array of holes around the azimuth of the profiled tip, typically there are 5 or 7 holes in total. Calibrated correctly, they will provide data up to a flow angularity of 60° or so, and will provide local static pressure p, stagnation pressure p_o and (u, v, w) velocity. Pressure transducers placed close to the probe tip will give the probe a frequency response of 1kHz or so, and these types of probes can be used for unsteady flow field measurement. Images of multi-hole probes are shown in Fig. 2.5, these are mounted on a traverse and moved around the flow field. Probes such as these only require one comprehensive calibration that remains valid so long as the geometric properties of the probe are not altered; the reader is referred to Shaw-Ward et al. [7] for a description of a calibration process for this type of probe.

Wake or Jet Rake. A wake or jet rake is an array of fine diameter stagnation pressure probes mounted on a streamlined support. The probes are spaced at regular intervals, and the rake may be as large as practically allowable. They replace the job of a single probe mounted on a traverse, but it might be mounted on a traverse for additional wake resolution or for a spanwise traverse. Some of the probes on the rake are static pressure probes, and data from the rake are integrated using momentum theory.

Surface Pressure Tapping. Body surface pressures are measured using a pressure tapping. This is a small hole $<$ 1mm diameter drilled into the model surface, this may then be connected to the pressure sensor. The model maker must be careful to ensure that the tapping is flush to the surface so that the tapping itself does not affect the local pressure. They must be at precise locations. There is always a compromise about the number of tappings that may be created, this may be due to space limitations

or the number of pressure sensors available. How the pressure sensor is connected to the tapping itself is an important issue; a long tube may be connected to a pressure scanner, but when unsteady pressure measurements are required the pressure sensor must be located as close to the pressure tapping as possible.

Pressure Scanner. Pressure scanners allow measurement of large pressure arrays. They have the disadvantage that they tend to be connected to pressure tappings or probe ends by long tubes, and cannot therefore be used for unsteady pressure measurement; this is not to say they cannot be used for unsteady pressure measurement, the user must be careful of the length of pressure tube connection and the performance characteristics of the scanner. They have the distinct advantage of flexibility of use, and should be regarded as an essential piece of laboratory equipment that offer tremendous value for money if looked after and treated well. Modern scanners allow reconfiguration of subsets of the scanner array, so that multiple pressure ranges are available within the same module.

Pressure Transducers. Pressure transducers are the small sensors that may be used to convert the pressure into a signal for measurement. Individual pressure transducers are typically mounted close to surface pressure tappings for measurements of time-varying pressure at the model surface; they may be very small indeed and have a bandwidth of tens of kHz, but the lower cost type have limited bandwidth and tend to be larger in size. Pressure transducer cost has reduced over the last few decades, so that instrumenting a test model with surface mounted pressure transducers and leaving them in the model does not carry such a high financial penalty. Figure 2.6 showing a pressure transducer array mounted in the inside of the model, once the model is closed up the transducers are irretrievable. Note that the connection tube length from the surface pressure tapping to the transducer membrane is critical; pressure signals are attenuated and their phase changes when connected to a pressure pipe, if the tube is too long the attenuation and phase change become excessive, and the tube short be as short as possible.

Large arrays of pressure transducers have to use high channel count data acquisition systems that are able to exploit the bandwidth of each individual transducer. Some pressure transducers have only very small output voltages, amplifier arrays are necessary, so a suitable signal conditioning and data acquisition system has to be available. Pressure transducers mounted inside rotors or propellers will have their output signal fed out of the rotating environment using a slip ring array.

Pressure Sensitive Paint. Pressure sensitive paint (PSP) works on the principle of the partial pressure of oxygen in air and its effect on a paint substrate on the model surface. Images of the model surface during a test are recorded. The PSP method has the advantage that the model does not have to be instrumented with pressure tappings or pressure transducers, but it works best at higher dynamic pressures. It has promise for helicopter rotors, where the dynamic pressure is high.

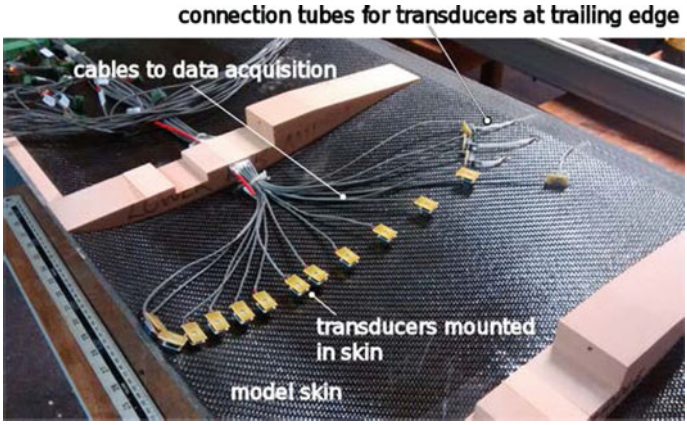

Fig. 2.6 Surface mounted pressure transducers mounted inside model (J. Walker, University of Glasgow, UK

2.7 Thermal Anemometry

Thermal anemometry includes the so-called hot-wire technique. It is an important method for flow velocity measurement, and it has the distinct advantage over all the other techniques of an exceptionally high bandwidth. Hot-wire probes are mounted on a traverse, and can be used for a wide range of flow fields if their operational requirements are understood. The technique is highly cost-effective in terms of the capital cost of the instrumentation, low maintenance costs, long shelf life of the parts, and should be present in any aeronautical laboratory. Thermal anemometry systems have various modes of operation, the one to be described further is that of constant temperature anemometry. The reader should refer to Ref. [1] and conduct thorough background reading on hot-wire theory and operation.

2.7.1 Theory of Thermal Anemometry

Figure 2.7 shows the basic principle of thermal anemometry; an electrical current heats a wire, convective heat transfer due to the flow speed U cools the wire down. A relationship between the flow speed and the electrical current must be established. In constant temperature anemometry, a control circuit keeps the wire at a constant temperature, and the wire voltage can be measured. The wire is typically very small diameter (a few microns) so that thermal inertia is low.

A wire is supported between prongs, the wire length might be 2mm or so. The flow speed U is at an arbitrary orientation to the wire, and the component of velocity driving the heat transfer is normal to the wire axis. Wires are arranged in pairs or as three to evaluate velocity components. A typical arrangement for a pair of wires is in the shape of an X (viewed from the side), where two slanted wires are arranged notionally at right angles with respect to one another.

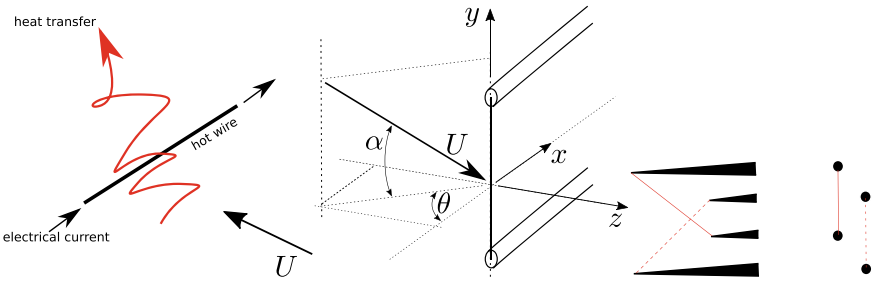

Fig. 2.7 Principle of thermal anemometry

2.7.2 Calibration

Calibration is an essential step for hot-wire anemometry. The established relationship between the wire voltage V and velocity U normal to the wire is through King's Law, $V^2 = A + BU^n$, where A, B, n are constants. Calibration is best done using a purpose built calibration rig that the wire is fitted into, this will generate a range of flow speeds and sample the wire voltage to evaluate the relationship. Cross-wires or triple wires are calibrated at known yaw and roll angles, so that the flow direction can be determined. Calibration does need to be done frequently, the wires get dirty for example.

2.7.3 Use of Hot Wires

The constant temperature anemometry technique may be used to evaluate the mean flow field, but it is particularly useful where turbulence quantities are required. The signal is continuous, and the measurement volume is small. Probes can be placed in difficult to access locations, and arrays of probes will provide data at many locations in the flow.

2.8 Flow Tracer Methods

Techniques for flow field measurement described so far all require the use of a probe. These have the disadvantage that the presence of the probe and its supporting apparatus may affect the flow field, and there is a wish to avoid this. Flow tracer methods rely on a tracer medium that follows the flow and may provide a signal that can be measured. They are most usually associated with flow field velocity

measurement, This section will consider the dynamics of a tracer particle, and an introduction to particle image velocimetry and laser Doppler anemometry will be provided.

2.8.1 Tracer Particle Dynamics in 1-D Flows

The tracer particle is fundamental in providing the signal to be measured, it reflects or scatters incident light. An analysis of the tracer particle dynamics in a fluid flow is informative, as it has a fundamental impact on the choice of instrumentation and the limitations of the technique; the experimentalist should not take it for granted that the tracer particle follows the fluid flow exactly. The reader is referred to Ref. [8] for a rigorous analysis of the dynamics of a flow tracer particle. We consider the motion of a small tracer particle of diameter d_p in 1-D flow of velocity u_f. In any tracer particle method, it is the particle velocity u_p that is measured. The particle does not simply follow the flow; the particle has forces exerted on it by the flow, and the particle accelerates in response to these forces. There is relative velocity $V = u_p - u_f$ between the particle and the fluid, and this is responsible for three of the forces acting on the particle as follows:

- Drag force D_p, this is the viscous drag force on the particle due to relative velocity V. For practical purposes the particle flow is a Stokes flow, for which a well known relationship exists;
- Force A_p required to accelerate fluid displaced by the particle. As the particle accelerates due to change of fluid velocity the mass of fluid displaced by the particle has to accelerate. It is a non-viscous force, and is easily modelled using potential flow theory;
- Basset history force B, which is a viscous force on the particle due to its unsteady motion. It is due to unsteady boundary layer development over the particle.

The remaining force P is due to pressure gradient in the fluid *in the direction of flow*. This is a streamwise buoyancy force. There are other effects on tracer particles due to pressure gradients in a flow, these will be discussed later. The equation of motion of the particle is then

$$\rho_p \frac{\pi d_p^3}{6} \frac{du_p}{dt} = -D_p - A_p - B + P. \tag{2.1}$$

Ref. [8] provides a detailed discussion of this equation. We are interested in the motion of a particle intended to follow the flow speed, we are not interested in a two-phase flow for example, so we suppose that our tracer particle is small. The Bassett history force may be neglected for most applications. A consideration of the particle response to a sinusoidal fluid flow speed u_f at circular frequency ω is useful to consider, then a transfer function H is defined such that

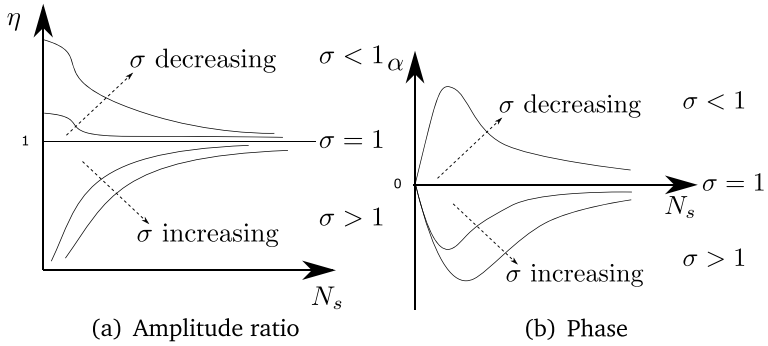

Fig. 2.8 Amplitude ratio η and phase α of particle response in sinusoidally oscillating fluid flow speed u_f as a function of Stokes number N_s

$$u_p(i\omega) = H(i\omega)u_f(i\omega). \tag{2.2}$$

We then define an amplitude ratio $\eta = u_p/u_f$ and a phase angle α. Summary sketches of the variation of η and α as a function of Stokes number

$$N_s = \sqrt{\frac{\nu_f}{\omega d_p^2}} \tag{2.3}$$

are shown in Fig. 2.8, where curves for different particle: fluid density ratio $\sigma = \rho_p/\rho_f$ are shown.

This reveals some fundamentally important observations as follows:

- Amplitude ratio is 1 and phase angle is zero for $\sigma = 1$. This means the particle follows the flow perfectly;
- *Heavy particle* has $\sigma > 1$, the amplitude ratio is less than 1, the phase angle is negative. The particle speed lags the flow speed;
- *Light particle* has $\sigma < 1$, the amplitude ratio is greater than 1, the phase angle is positive. The particle speed leads the flow speed.

The optimal particle has $\sigma = 1$, it is neutrally buoyant. The change of behaviour either side of $\sigma = 1$ is due to the streamwise buoyancy. The choice of testing medium has a significant outcome on the availability of tracer particles as follows:

- Wind tunnel. Air density is typically $\rho_f = 1.225\ \text{kgm}^{-3}$. It is extremely difficult to arrange for a neutrally buoyant particle; a gas filled bubble is possible, but is it practical?—Significant progress has been made with the use of helium filled soap bubbles, the technique is now viable. Furthermore, suitable particle substrates will be significantly denser than air. Tracer particles for air and gas flow measurement have $\sigma \gg 1$.
- Water tank. Water has density $\rho_f = 1000\ \text{kgm}^{-3}$, there is a wide choice of particle substrate than can give $\sigma \simeq 1$.

Given that the requirement is that the tracer particle is required to follow the flow speed as closely as possible, experimentation in water as a fluid medium seems ideal. This is indeed the case, and water offers other benefits such as higher hydrodynamic forces, but water as a testing medium presents practical challenges that are difficult to overcome. We will restrict the discussion to problems appropriate for wind tunnels, but the experimentalist must be aware of the challenges specific to the testing medium.

Tracer Particle for Air Flow. We have established that we must accept a tracer particle density ratio $\sigma \gg 1$ for an air flow. Take Eq. 2.1 for the 1-D motion of the particle, an order of magnitude analysis then means that the particle Stokes drag D_p is the dominant term on the right hand side, so we solve

$$\rho_p \frac{\pi d_p^3}{6} \frac{du_p}{dt} = -3\pi \nu_f \rho_f d_p V. \tag{2.4}$$

Solution of Eq. 2.4 is straightforward, and we can consider two types of fluid flow as follows:

Sinusoidally Driven Fluid Flow. Consider a sinusoidally driven fluid flow speed u_f at circular frequency $\omega = 2\pi f$, we have a phase difference $\tan\alpha = \omega/C$ and particle: fluid amplitude ratio

$$\eta = \left(1 + \frac{\omega^2}{C^2}\right)^{-1/2}, \tag{2.5}$$

where $C = 18\nu_f/\sigma d_p^2$. A calculation for an air flow with $\sigma \approx 1000$, $d_p = 1$mm, $\nu_f = 1.5 \times 10^{-5}$ reveals negligible phase difference and very high amplitude ratio ($\eta > 0.99$) up to frequency around $f = 6$ kHz.

Step Change in Fluid Velocity. Solution is straightforward for a step change in fluid velocity from one constant value (e.g. $u_f = 0$) to another, e.g. $u_f = U$. We then have the solution

$$u_p(t) = U\left(1 - e^{-t/C}\right). \tag{2.6}$$

The particle speed approaches the fluid speed asymptotically. It is useful to consider $t_{0.99U}$, the time the particle takes to accelerate to $u_p = 0.99U$, then

$$t_{0.99U} = -C \log_e 0.01. \tag{2.7}$$

Fig. 2.9a shows physical particle response time for a range of density ratio σ up to $d_p = 100\ \mu$m.

Due to the square relationship with d_p the response time becomes large as d_p becomes large. The question is, how quickly should a particle respond? A meaningful time scale is c/U, where c is, for example, a chord length, so a meaningful time response must be significantly smaller than this. The purpose of a tracer particle is to

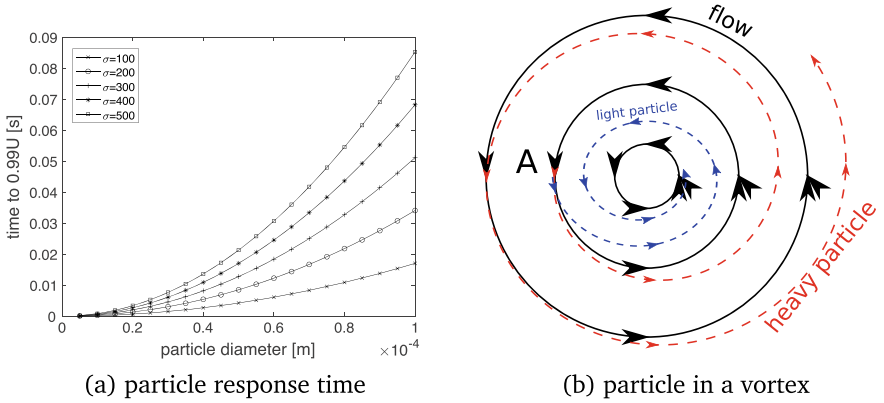

(a) particle response time (b) particle in a vortex

Fig. 2.9 Tracer particle dynamics. **a** particle response time to reach 0.99 of step increase of fluid velocity U; **b** particle trajectory in a vortex flow, particle released from point A

provide the velocity information at that location, so the answer is that the response time should be as short as possible. A typical seeding substrate for a flow in air is oil with $\sigma = 660$, then a particle diameter of 1 micron gives $t_{0.99U}$ of about $11\mu s$. A 10 μm diameter particle has a response time $\sim 10^2$ times larger; this *may* be regarded as acceptable according to this analysis, but there are other issues to consider which will be discussed next.

Behaviour of a Tracer Particle in a Curved Flow Field. So far we have considered a 1-D flow only. A feature of a 2-D or 3-D flow is flow field curvature. Consider a 2-D vortex flow, we are interested in the tangential velocity u_θ. There is a radial pressure gradient

$$\frac{\partial p}{\partial r} = -\rho_f \frac{u_\theta^2}{r} \tag{2.8}$$

that maintains the rotation, this is exactly sufficient to accelerate the fluid parcel such that it follows the curved path. Now consider the force required to make the particle follow the circular path around the vortex centre. The speed u_θ is constant, but the flow is accelerating everywhere in space due to the continuous change of direction. The step response calculation shown in Eq. 2.4 is not useful. A *fluid parcel* of notional diameter d_p requires force $\pi \rho_p d_p^3 u_\theta^2/6r$ to follow the circular path, and this is provided by the radial inward pressure gradient in the fluid. A *tracer particle* of notional diameter d_p requires force $\pi \rho_p d_p^3 u_\theta^2/6r$ to follow the circular path, but the radial inward pressure gradient in the fluid cannot provide this force in the case $\rho_p > \rho_f$, and the particle accelerates radially outward. Conversely in the case $\sigma \ll 1$ the force provided by the fluid radial pressure gradient exceeds the centripetal force required by the particle, and the particle accelerates radially inward. Figure 2.9b shows the trajectory of a heavy and a light particle in a vortex flow, the heavy particle moves outward as it orbits the vortex centre, the light particle moves inward as it

orbits the vortex centre. In wind tunnel flows, this means that vortices are spotted easily by particle seeding voids at their centres. In addition to the uncertainty about velocity measurement accuracy, there is information loss where the particle seeding void exists.

To extend this analysis, we may suppose that the particle reaches a particle radial velocity u_{pr} in the vortex, then for $\sigma \gg 1$ the Stokes drag force in the radial direction balances the centripetal force for the particle, then

$$\frac{\pi \rho_f d_p^2}{6} \frac{u_\theta^2}{r} = 3\pi \nu_f \rho_f d_p u_{pr}, \tag{2.9}$$

Thus

$$u_{pr} = \frac{\sigma d_p^2}{18\nu_f} \frac{u_\theta^2}{r}. \tag{2.10}$$

The terminal radial velocity u_{pr} is reduced with a very small particle diameter d_p. Consider an air flow with a vortex with $u_\theta = 20\text{ms}^{-1}$ at r =0.05m. The 1 micron diameter particle with $\sigma = 660$ will have $u_{pr} = 0.02\text{ms}^{-1}$. While there will be a seeding void due to higher acceleration at younger vortex age, this represents a negligible error in terms of velocity magnitude, but radial velocity measurements must be treated with caution.

Tracer Particle for a Wind Tunnel Flow. Much experience has been gained over decades of wind tunnel testing work using particle tracer methods. We have to accept that $\sigma \gg 1$, the particle will be heavy. To compensate for this so that the particle dynamics do not deviate excessively from the fluid dynamics, the tracer particle must be very small indeed. 1 micron is typical, with oil (e.g. olive oil) or water based solutions (polyethylene glycol) as the substrate. Even smaller particles include substances such as TiO_2, where particle size is around 200nm, and these may be used in supersonic flows for example. Great caution must be taken with aerosol leakage, as sub-micron particles can enter the bloodstream directly through the lungs. The reader is encouraged to search the literature to gain a wider awareness of seeding tracer particles for wind tunnels, what is already available should not be taken for granted.

2.8.2 Optical Characteristics of Tracer Particles

We observe that a tracer particle in an air flow has to be extremely small, around 1 micron, for it to follow a fluid flow with an acceptably small error. By definition, methods using tracer particles rely then on reflection or scattering of light. Lorentz-Mie theory presents a solution of Maxwell's equations for the interaction of electromagnetic radiation with a sphere. Ref. [9] deals with this aspect of a flow tracer particle, and the reader is referred to this book and should read wider. The results

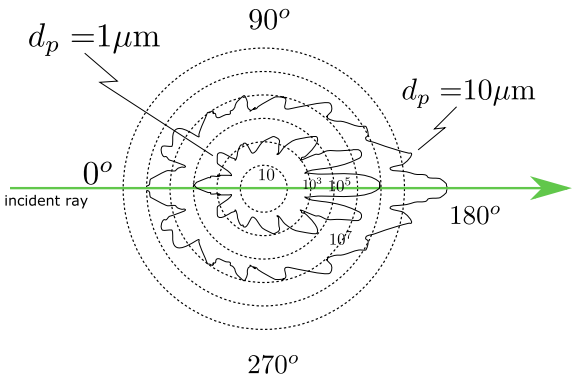

Fig. 2.10 Sketch of light scattering power (dashed circles indicate levels with powers of 10) as a function of direction for 1 micron and 10 micron particle size. Sketch is approximate [9]

are key and have significant implications for the instrumentation requirements. A small particle does not simply reflect light. We cannot simply consider scattering of light by particles as a simple reflection problem. From a basic perspective light will diffract around a small particle, some light will be reflected off the surface and the light that passes into the particle will be refracted and suffer many internal reflections until it then passes out of the particle. The number of internal reflections depends on the Brewster angle, and this is the incident angle at which light will pass through a refractive index interface. When viewed from a particular scattering angle, therefore, a light ray may notionally have followed a number of beam paths, and the intensity of the scattered light will vary strongly as a function of the scattering angle. Furthermore when the particle is sufficiently large constructive/destructive interference of light waves will take place within the particle, and therefore the light intensity will vary considerably with the scattering angle, with lobes of high intensity being a distinctive feature of the scattered light. It is useful to consider thin film interference as an example to help understand this.

A sketch of the Mie scattering profile for particles of 1 micron and 10 microns is shown as Fig. 2.10. There are two key points from this:

- Scattered light power increases enormously with increase of particle size d_p;
- Scattered light power changes remarkably dependent upon scattering direction. Forward (180°) and backward (0°) scatter directions provide the highest power, while scattering to the side is orders of magnitude lower.

The latter point is demonstrated easily using a laser pointer; the beam is difficult to see from the side, while it is easy to see viewing at a direction close to the axis (point the laser way from your eyes!). The scattering behaviour explains the layout of laser Doppler systems and drives the pulse energy requirements for lasers for particle image velocimetry. Particle size effects mean that optical methods with tracer particles are particularly well suited to flow measurement in water, as the demands on instrumentation performance are less. All of this is driven by the need for flow tracer particles to be small, and especially small for flow measurement in air where

$\sigma \gg 1$. Lasers tend to be used for specific experimental methods because they are capable of providing the intense illumination required and can be directed with great precision. Successful experimentation in water is possible using other light sources. Flow visualisation of smoke plumes can be done using floodlights or strobe lighting.

2.8.3 Particle Image Velocimetry

Particle image velocimetry (PIV) has emerged as one of the most important and powerful techniques for flow field measurement. Its operating principle is straightforward, and it provides the researcher with data that can provide a deep understanding of the behaviour of a fluid flow because it can provide velocity information over a wide part of the flow field at a near instant. It is especially well suited to unsteady, separated flows where transient phenomena occur. Its ubiquity in laboratories can act as a double-edged sword, however; it can be used in an inappropriate manner, for example measuring a flow using PIV becomes a goal of its own, and more informative techniques are forgotten about. The researcher needs to justify why PIV should be used, flow field information is only useful in support of other data. PIV for wind tunnels has the distinctive disadvantage that the instrumentation is extremely expensive. The inexperienced researcher will be misled by the apparent ease with which the commercially available PIV systems work, and it is a depressingly common occurrence that neophyte PhD students are allowed to walk into a laboratory knowing neither how to focus a camera nor calculate a PIV time delay. There is no substitute for understanding the technique, and the user manual of an off-the-shelf system is not the way to do this. PhD student supervisors who allow their students to enter a laboratory without thorough background knowledge and adequate training need to take note that they are exposing their students to great risk of personal harm due to the use of class 4 lasers, and the likelihood that very expensive instrumentation will be damaged beyond repair. In many respects an experimental campaign using PIV should be the *last* item on a list.

This section will describe the basic operating principle of PIV. The reader is referred to the book by Raffel et al. [9] and should read around the subject widely. In particular the reader should follow the development of PIV over the last few decades; what might now take a few seconds to compute in a laboratory will have taken many days of effort in the 1980s. The PIV practitioner needs a good understanding of optics and photography, be familiar with the theory of operation of lasers and their practical implementation, understand elements of signal and image processing, and have a fine dexterity and enormous reserves of patience.

Basic Principle of PIV. In its most basic form, PIV gives two component velocity field (u, v) in a plane (2D2C). Stereo PIV gives three velocity components (u, v, w) in a plane (2D3C). Both these methods infer the velocity from particle displacement in the measurement volume projected onto a recording medium, the measurement plane most usually defined by a very thin laser light sheet. Tomographic PIV will

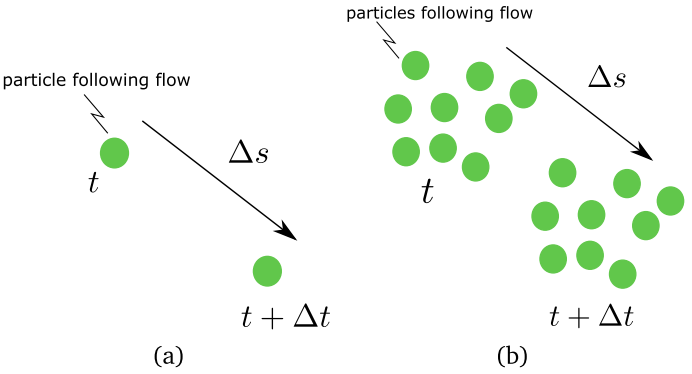

Fig. 2.11 Schematic diagram of basic operating principle of PIV: **a** basic principle and **b** movement of cluster of particles

give three velocity components (u, v, w) in a three dimensional volume (3D3C). *Never* attempt either stereo or tomographic PIV without first becoming competent in the use of 2D2C PIV.

Figure 2.11 shows a schematic diagram of the basic operating principle of PIV. The particle indicated at time t moves with the flow to the location at time $t + \Delta t$, the displacement is Δs. Velocity is defined as

$$\underline{V} = \lim_{\Delta t \to 0} \frac{\Delta \underline{s}}{\Delta t}, \tag{2.11}$$

Thus, PIV attempts to determine velocity directly and not by some other physical effect that can be measured. It needs to be understood that PIV provides velocity information over a finite but short time interval. The challenge with PIV is to determine the displacement vector $\Delta \underline{s}$. Δt is the PIV time delay; this needs to be short enough to satisfy the definition of velocity without excessive error, but long enough to determine particle displacement Δs with sufficient accuracy.

Ideally, each tracer particle in the flow is tracked individually, which would require each and every particle to be identified. In principle this is a good approach, but it is computationally awkward. Another matter is how particles are imaged. We know that a guideline particle size for a flow in air is 1 micron, optical wavelengths of light are then of the order of the particle size (a frequency-doubled Nd:YAG laser commonly used for PIV has a wavelength of 532 nm), so particle imaging is diffraction limited, and this is compounded by the spatial resolution of camera sensors. There is significant information loss about the particle. A practical approach to PIV is to seed the flow with many particles and use cross-correlation to track the movement of a pattern of particles, which has the advantage that individual particles do not have to be identified and the cross-correlation process is well understood. Figure 2.11b shows this notion. An image of a wide area of the flow field allows particle tracking or cross-correlation to be performed over the entire image by interrogation over small regions of the image, so that a picture of the flow field is built up.

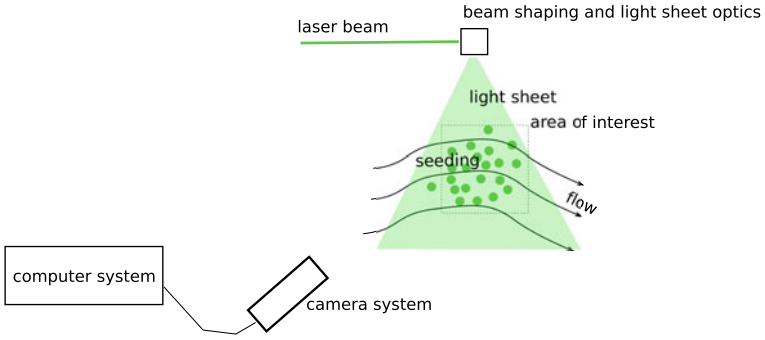

Fig. 2.12 Schematic diagram of the fundamental components of a PIV system arrangement

Instrumentation for PIV. This short section outlines what is required for a PIV experiment. It assumes the experiment has been set up and that optical access is available within the wind tunnel. The functioning of each component is critical, and the user must be familiar with the specification and functionality of each system component. A simple layout of a system set up for PIV is shown in Fig. 2.12.

Particle Seeding. This is the most fundamental element of the instrumentation. The seeder must be able to provide seeding for the wind tunnel at a sufficient rate, the larger the wind tunnel, the higher the seeding generation rate. Typical seeders use arrays of Laskin nozzles that atomise an oil substrate (e.g. olive oil), so a good compressed air source is required. Systems that heat mineral oil to create a mist that is pumped into the wind tunnel are also used. Oil can make a mess of the wind tunnel. DEHS can be used in these seeders, and alternatives include fog generators most normally used in the entertainment industry.

Illumination. For wind tunnels the most common illumination source is the pulsed Nd:YAG laser. The user must understand the laser arrangement and how the laser works, as a frequent source of problems is with the laser. The laser beam is delivered into the working section by a suitable arrangement of optics, a telescope to control the beam diameter, and the laser beam is expanded by a cylindrical lens into a thin sheet in the working section of the wind tunnel. All optical surfaces must be kept clean, all access windows must be blemish and scratch free. The user needs to know the flow area to be imaged beforehand, and be able to guide the light sheet into the correct position avoiding shadow as much as possible. This is a very difficult process that requires care and patience as class 4 lasers are usually involved. Tips and tricks include use of fluorescent tape and pens so that the laser can be seen through laser safety goggles.

Camera System. The size of the field of view that can be recorded successfully for PIV depends upon the laser power available and the camera resolution. These components need to be matched carefully. Cameras must be fitted with high quality lenses that can be focussed at the required stand-off distance and have a good enough f-number for image intensity. The user must be able to align the camera with the

required field of view and focus the camera. Cameras for PIV have triggering and synchronisation inputs that have to be connected to the laser timing and computer system correctly, if this is not understood and done correctly much time will be wasted.

Computer System. The computer system controls the entire PIV system including the laser and camera timing. A modern PIV system can easily produce terabytes of data in a very short amount of time, so it must have significant storage capacity. *Never* use the wind tunnel PIV computer for bulk data analysis, as that will prevent the wind tunnel control room being used for other tasks. PIV processing should be done off-line on a separate computer system.

Spatial Calibration. Spatial calibration of the PIV system is an essential step. The camera used for PIV records the images as a pixel array, but the flow being measured is in physical space. Part of the experimental procedure is to record an image of a calibration grid at the same location as the PIV laser light sheet. The calibration grid is a known pattern, usually a pattern of dots on a contrasting background, and dot pitch is known precisely. A calibration grid of appropriate size is required. The calibration process provides the user with important information about the size of the field of view that can be recorded, and this information, along with knowledge of the flow speed and camera sensor resolution are required for calculation of the PIV time delay Δt.

Performance and Accuracy of PIV. A general rule for any experiment using any technique is to assume in the first instance that the results are not correct. They need to be checked carefully. The most common experience of researchers will tend to be through the use of a commercial PIV system, the mistake then is to assume it will do everything; they do not, and cannot in any way compensate for lack of knowledge of the user. PIV is very good at giving the user misleading data, and the user must be able to understand (1) the basic quality (fidelity) of the data from a PIV experiment and (2) the accuracy of a valid measurement. The only way to evaluate this is to have a thorough appreciation of the principle behind PIV, and to have done comprehensive background reading and, ideally, performed some numerical experiments using a PIV training utility. Data should be reviewed using a fresh pair of eyes, something obvious may emerge. At risk of provoking controversy, the accuracy of PIV can tend to be overstated. A realistic expectation is that PIV is a good tool for quantitative flow visualisation, and the most important aspect then is the fidelity of the result. The user needs to be familiar with:

- Random and systematic bias errors. A keen understanding of the instrumentation performance is the key to an appreciation of the latter. So-called peak locking in digital PIV is a bias error that all PIV users need an awareness of.
- Spatial resolution and over-sampling. How do the PIV analysis parameters affect the actual measurement resolution? Does over-sampling increase the measurement resolution?
- How do the vector validation methods employed work? What is their effect on the result?

The risk is that the user can overstate the capabilities of the system.

Post-processing of PIV Data. PIV provides a velocity field. What is subsequently done with those data depends upon the research goals. A common theme in this chapter is the advice that the researcher should understand the theory behind a technique, and for data post-processing this means an awareness of the mathematical demands for analysis of the type of discrete data that PIV provides. Simply using a function supplied with a system is not a good approach, as it may in fact be inappropriate. A good example of this is numerical differentiation for vorticity, for example; what is the best way of differentiating the data? A sequence of PIV images will allow mean flow and some statistics to be calculated; how many PIV images are required, and what do those statistics mean?—PIV provides snapshots of the flow, and this lends itself to a modal analysis, for example proper orthogonal decomposition (POD). A POD analysis will provide a set of modes whatever data are provided, but what do these modes mean?

Stereoscopic PIV. The basic 2D2C approach in PIV gives a notional (u, v) velocity in an (x, y) plane. Occasionally the three component velocity field (u, v, w) is required, where w is the velocity component normal to the measurement plane. This might be because the w component contains useful information, or perhaps the researcher is forced to use oblique viewing angles due to optical access issues. The particle displacement computed in PIV is from the projection of the particle movement in the volume of interest onto the recording medium. The reader is referred to the article by Prasad [10]. The projection of the recorded movement onto the focal plane coincident with the light sheet permits a relatively straightforward analysis of the perspective effect, and this is shown in Fig. 2.13. The most obvious camera view alignment is at a direction normal to the measurement plane, and perspective errors are negligible unless a wide area at short stand-off distance is being recorded. The difference in perceived particle displacement due to an oblique viewing angle is depicted in Fig. 2.13; the displacement perceived at oblique viewing angle θ is quite different from that of the normal view.

In stereo PIV, two PIV cameras are set at oblique viewing angles, usually at positive and negative θ relative to the normal, and the ideal angle between the two cameras is 90° or so. A rectangle viewed off axis becomes a trapezium, so there is significant distortion to be taken care of in the stereo processing methodology. Focussing the PIV cameras is a challenge, because the object plane is no longer normal to the lens principal axis so only a limited width of the light sheet comes into focus. A high lens f-number will increase the depth of field at the expense of less light entering the lens, but the usual approach is to use a so-called Scheimpflug mount that allows the lens and camera sensor axes to be tilted with respect to one another to give sharp focus across the field of view. Particularly careful focussing and calibration steps are required for stereo PIV, this allows the image distortion due to the off-axis view to be compensated for, and the stereo viewing angle for the stereo reconstruction may be computed. The process of setting up the instrumentation is much more difficult, and the data processing burden is more than twice that for two-component PIV. It is

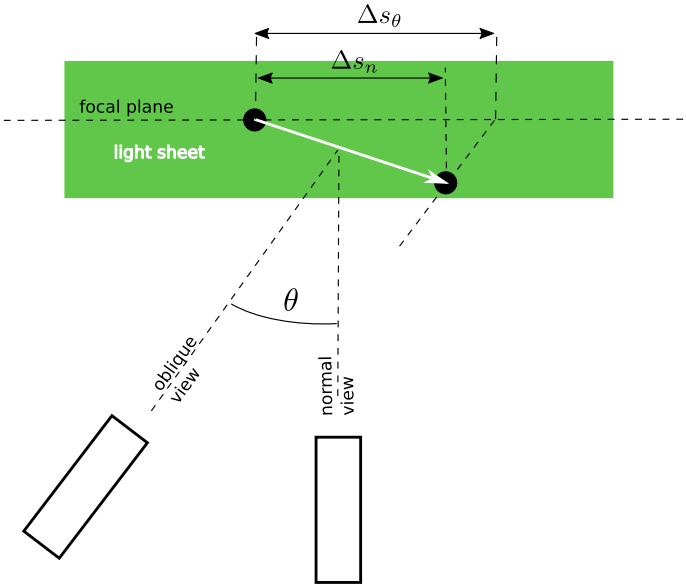

Fig. 2.13 Normal and oblique camera view at angle θ with PIV. The perceived particle displacements are Δs_n and Δs_θ respectively

for these reasons that the researcher should be very careful about the need to conduct stereo PIV in the first place, and only then to attempt it after sufficient experience with basic PIV has been gained.

2.8.4 Laser Doppler Anemometry

Doppler effect is a wave phenomenon in physics that is understood well. The laser Doppler anemometry method (LDA) came into being in the 1960s, as the development of the laser made an optical technique based upon Doppler effect a possibility. The reader is referred to Ref. [11] as a springboard for wider reading into the technique. As the technique relies on flow tracers, the requirements of the tracer particles are the over-riding concern (small diameter for gas flows). In turn this drives the specifications of the instrumentation.

Basic theory of LDA. Incident light illuminates the particle, and scattered light is picked up by a detector (the receiver). Doppler effect depends on the relative orientation of the incident light and the receiver, and the Doppler effect is invoked twice, firstly when the light hits the particle, and secondly when it is scattered to the receiver. It is essential that the reader understands the Doppler effect and how it is used in a practical LDA system.

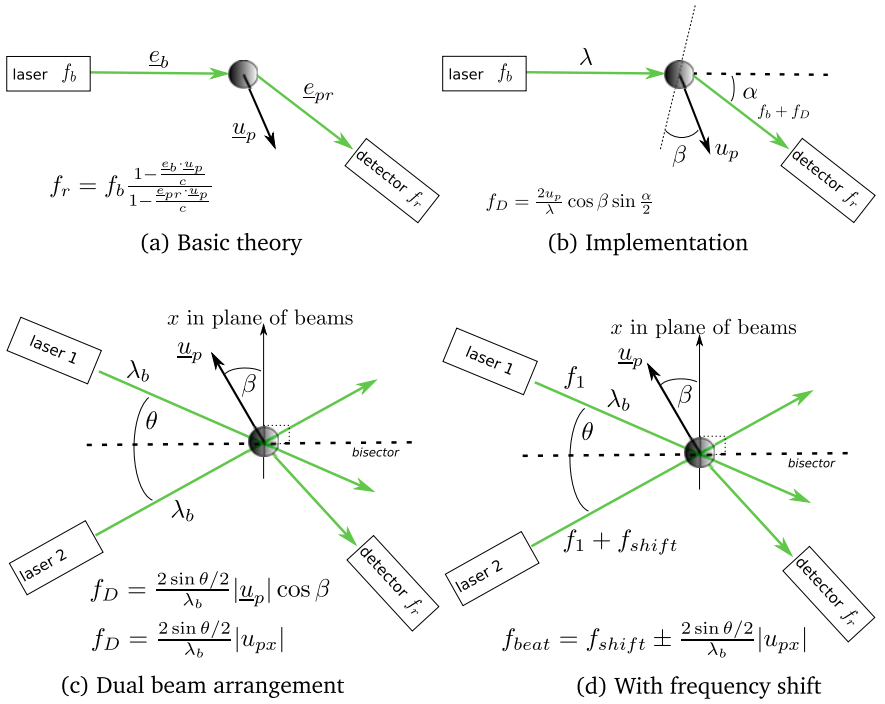

Fig. 2.14 Schematic diagram of transmitter (laser) and detector (receiver) with Doppler effect due to particle moving at velocity $\underline{u}_p$

Figure 2.14 shows an arrangement of a laser and receiver and how the Doppler effect theory is applied, with an illustration of the Doppler shift frequency and its dependency on the arrangement of the components and the direction of the particle motion. Note that in this sketch the receiver optic is arranged in a forward scatter direction to take advantage of the higher intensity of forward scattered light according to the Mie scattering theory. A typical laser for LDA has wavelength around 532 nm, therefore frequency $f_b = 5.6 \times 10^{14}$ Hz. Doppler frequency shift is typically less than 4 MHz per unit speed u_p, so the Doppler shift is less than one part in 10^8. This is tremendously difficult to measure, and a common implementation is to use a second laser beam with different incident direction and hence different Doppler shift. This is shown in Fig. 2.14 graphs (c) and (d), where the two beams coincide at a point. There is different Doppler shift frequency due to the different directions of the incident beams relative to the receiver, and the difference between the two Doppler shifts is indicated in graph (c). Note that the frequency difference does not depend upon the angle of the detector relative to the laser sources, only to the bisector angle θ. The sense of velocity detected is defined by the plane of the two beams, and the velocity component sensed by this arrangement is u_{px} in the direction x in the plane of the two beams normal to the bisector line between the two beams. The difference in Doppler

shifted frequency f_D manifests at the detector as an optical heterodyne, a beating, and this can be measured. The problem remains that the direction of the velocity u_{px} cannot be resolved. If one laser is frequency shifted by f_{shift} with respect to the other, as in frame (d), then given that the detector is still individually sensitive to the relative directions of the incident beams, the beating frequency detected is biased by the shifted frequency, so that the beating frequency detected reveals the direction of velocity.

The reader is encouraged to follow the mathematics. The detected velocity u_{px} depends upon the beat frequency f_{beat} detected, the shift frequency f_{shift} imposed, the wavelength λ_b of the laser light, and the beam separation angle θ. Thus with high performance electro-optic components and with knowledge of the angle θ, the device needs no calibration, and accuracy is fundamentally high. If set up correctly, the LDA output will be unambiguous. A convenient model of the frequency shifted, dual beam LDA that the reader may consider is the so-called fringe model of LDA, where the tracer particle moves across a moving interference fringe pattern in the measurement volume defined by where the two beams coincide. A mathematical model of this gives the same result as the Doppler effect analysis, and it is almost as if the method is a time-of-flight technique. Whichever is used as a preferred description, the fundamental physical effect that the detector responds to is a time-changing intensity caused by interference. If there is any optical surface in any beam path that affects the polarisation state of the incident or scattered light, the interference effect will be extinguished; LDA cannot be expected to work reliably, for example, if there are any laminated or toughened glass, perspex or polycarbonate windows in the beam path. This is why a fundamental understanding of the LDA technique and its implementation are essential.

Typical laboratory implementation of LDA. Laboratory LDA systems take on many guises. The user has the freedom to tailor the system set up to match an experiment. The fundamental components are the lasers, the laser beam probe delivery heads, detectors and analysers and traverse system.

- Class-4 lasers are typically used;
- A typical modern laboratory will have the lasers fed into the optical heads by optical fibre;
- Some arrangements have the detector in the same probe unit as the laser delivery head, this exploits back scatter and makes for a very compact arrangement. Otherwise the detector might be in a different module;
- A two-component probe will take two sets of lasers. The beam pairs are arranged at right angles to allow the probe to measure two components of velocity. The actual physical velocity measured relative to wind tunnel axes then depends upon the direction of the probe axis, and that is the user's choice;
- Three components of velocity at a point may be measured by arranging three single component LDA probes or one dual component and one single component probe and bringing them to focus at a precise point. The angles of the probe axes relative to one another need to be known;

- Tracer particles arrive in the measurement volume at irregular intervals, as a particle passes through the measurement volume it emits a burst, and the burst spectrum analyser processes the signal and determines the LDA velocity during the burst.

Running an LDA Test. A wind tunnel and other experimental systems need to be run for a long duration in an LDA test. The researcher needs to be aware of a few key points.

- Do not be too ambitious with the number of measurement points early on in a test campaign. Higher spatial resolution scans can target areas of interest later on.
- Ensure the LDA traverse has the freedom to move over the planned scanning volume.
- Anticipate where the LDA beams may be blocked, and where strong reflections may occur.
- Do not allow LDA burst (count) rates to drop to too low a level, wind tunnel or test chamber seeding will have to be topped up.
- For dual beam LDA, check laser power levels are well-balanced while setting up the system. Check the balance as frequently as possible.
- Monitor the LDA performance during a test.

2.9 Case Studies and Results

We conclude this chapter with a short selection of experimental studies involving helicopter rotors and in some cases the complete vehicle.

2.9.1 Forces and Moments on a Model Helicopter Near an Obstacle

Helicopters frequently operate close to the ground and to buildings, the flow around the rotor is influenced by the presence of both. Figure 2.15 shows a helicopter model in a wind tunnel close to an obstacle on the ground [12]. The rig is in a large wind tunnel, and the helicopter model has a force balance on the end of the sting. The helicopter model contains a six axis load cell. The model was moved around using the traverse system supporting the model. The orientation of the helicopter model relative to the obstacle has a significant effect on the rotor forces and moments. The thrust data are plotted on the right; Z is vertical height of the model above ground. The test cases are T3 rotor in symmetry plane of obstacle and T4 a rotor facing an obstacle edge.

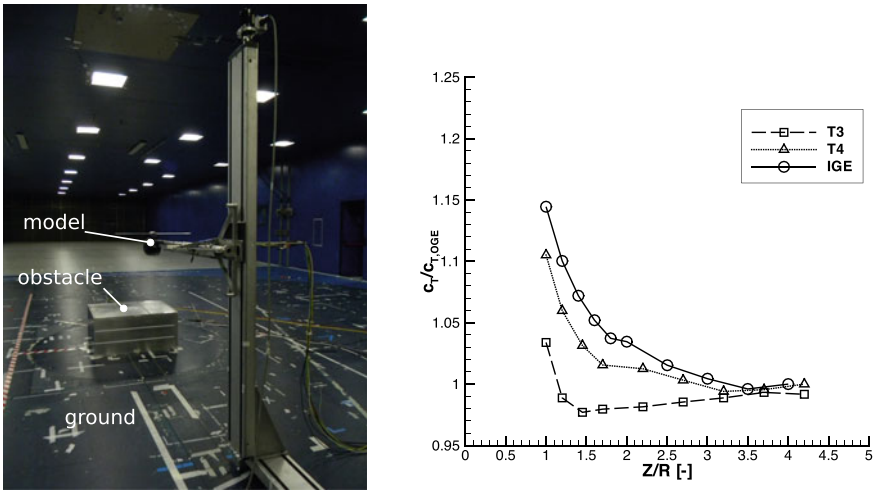

Fig. 2.15 Helicopter model close to an obstacle [12]. (D Zagaglia, Politecnico Milano, IT, 2016)

2.9.2 Dynamic Stall: Surface-mounted Pressure Transducers

Wind tunnel test campaigns for dynamic stall include experiments with models instrumented with surface mounted pressure transducers. Figure 2.1b shows such a test model. Sample data are shown in Fig. 2.16, from Ref. [13], where the development of the surface pressure distribution over the pitching cycle and the quarter chord pitching moment are shown. Surface pressure data show the build up of leading edge suction, its collapse and generation of the dynamic stall suction ridge, and the re-establishment of the fully attached flow. Pitching moment data are from integration of the pressure data.

2.9.3 Inflow to a Rotor: Flow Measurement with LDA

LDA measurements of a hovering rotor were performed, rotor diameter 1m. LDA was used to scan the inflow at a distance 1cm above the rotor disc. This was part of a study on the behaviour of rotor systems and rotor wakes in the vicinity of a neighbouring obstacle. Figure 2.17 shows the inflow velocity, positive into the disc [14]. Measurement of the hover inflow was compared with the flow in the presence of an obstacle beneath a portion of the rotor disc, and a load cell was used to determine thrust and trim state (Data from GARTEUR AG22 [15]).

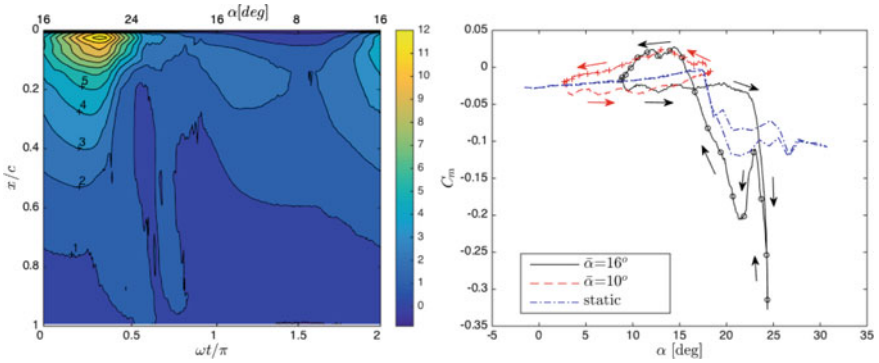

(a) Surface $-C_p$ (b) Pitching moment

Fig. 2.16 Dynamic stall measured using surface mounted pressure transducers. Sinusoidal pitch oscillation at reduced frequency 0.103, pitch amplitude 8^o, mean angle $\bar{\alpha} = 16^o$, Re $= 1.5 \cdot 10^6$ (Y. Wang, University of Glasgow, UK, 2007 [13])

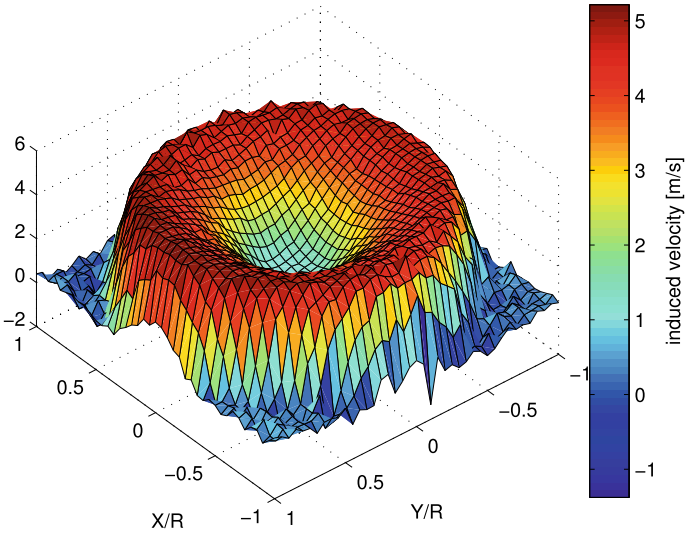

Fig. 2.17 LDA measurement of inflow induced by a hovering rotor; positive sense into the disc (D Zagaglia, University of Glasgow [14])

2.9.4 Smoke Flow Visualisation and Pressure Measurement

Smoke flow of the wake of a rotor hovering above a cuboid obstacle were performed [16]. If the smoke wand is placed close enough to the edge of the rotor disc, the smoke is entrained around the trailed vortex filaments. These filaments are persistent, and the smoke will reveal the helical vortex wake for several revolutions before the smoke is diffused or the wake breaks down. Figure 2.18 shows an image from a

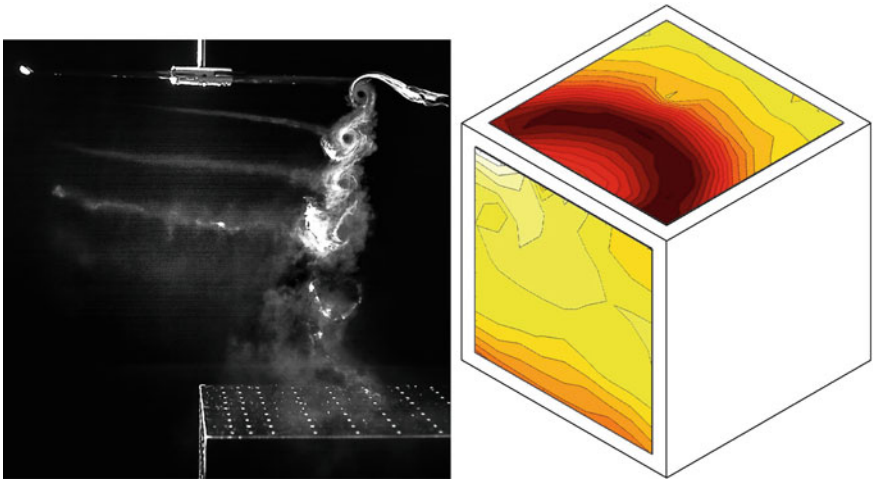

(a) Smoke flow (b) C_p contours on obstacle

Fig. 2.18 Rotor hovering at height 1 diameter above the edge of a cubic obstacle. (D Pickles, University of Glasgow [16])

flow visualisation sequence recorded by a high speed camera. Illumination was by stroboscope, strobe frequency was slightly different to rotor frequency to reveal the flow development in time in a strobed sense.

The graph 2.18a shows flow visualisation using a smoke wand with stroboscope. The smoke wraps around the vortex cores, and the trailed vortex filaments can be seen, these filaments impinge on the surface of the obstacle at the bottom right of the picture. The white dots are pressure tappings on the top of the obstacle. The graph 2.18b shows pressure contours from pressure messurements, colours are positive, the top surface of the obstacle supports half the rotor thrust in this case.

2.9.5 PIV of Rotor in Ground Effect in Forward Flight

A 1-metre diameter rotor system [17] was sting mounted in a wind tunnel over a rolling ground, ground speed matched wind tunnel speed. The rotor system was mounted on a balance, and cyclic inputs allowed the in-plane moments to be trimmed out. Stereo PIV was performed over a 1m wide area, seeding is olive oil, 1 μm particle size, relative density $\sigma = 800$. Data are plotted in Fig. 2.19, which shows an instantaneous vector field. The centre of is rotor at coordinates $(0, 0)$, the ground is at $y/R = -1$. The noisy w contours for $x/R > 2$ are due to edge of light sheet effects.

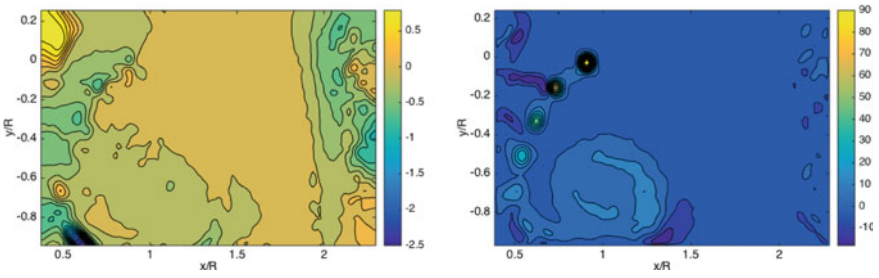

(a) w velocity (b) w in-plane vorticity

Fig. 2.19 Stereo PIV of a rotor in forward flight ground effect; normalised advance ratio 0.66. 1 m wide field of view, wind tunnel flow is from right to left. (N. Nathan, University of Glasgow; data from GARTEUR, Ref. [17]

Much effort was made with the stereo PIV, but the w-component data were of limited value. Noisy w data on the right hand side of the graph 2.19a are from edge of light sheet effects (low intensity). So errors are larger. Vorticity in graph 2.19b shows strong positive vorticity of the trailed vortex filaments, the roll up of these filaments into the distinctive ground vortex, and negative vorticity is from the separation induced at the ground by the ground vortex.

2.9.6 PIV of Rotor Vortex Ring State

These figures demonstrate the remarkable breakdown of the usually expected helical trailed vortex wake into the *vortex ring state* (VRS) under certain conditions of descent. PIV measurements were taken of the flow around a rotor towed along a long towing tank to simulate the descent [18]. Seeding material used was silver coated microspheres, particle diameter 100 μm, relative density σ =0.9. Rotor thrust was measured simultaneously so that flow field state could be correlated with thrust phase. Figure 2.20 shows out-of-plane vorticity and instantaneous streamlines around low thrust and high thrust.

The experiments have been carried out in water with time-resolved PIV and simultaneous thrust measurement. The leading edge of rotor disc is shown. The rotor centre is set at coordinates (0, 0). The positive vorticity trailed from the rotor tip and the negative trailed from rotor root. The VRS is characterised by the formation and shedding of a toroidal vortex that contains the entire rotor. This vortex system is formed from vortex system trailed from the rotor tip.

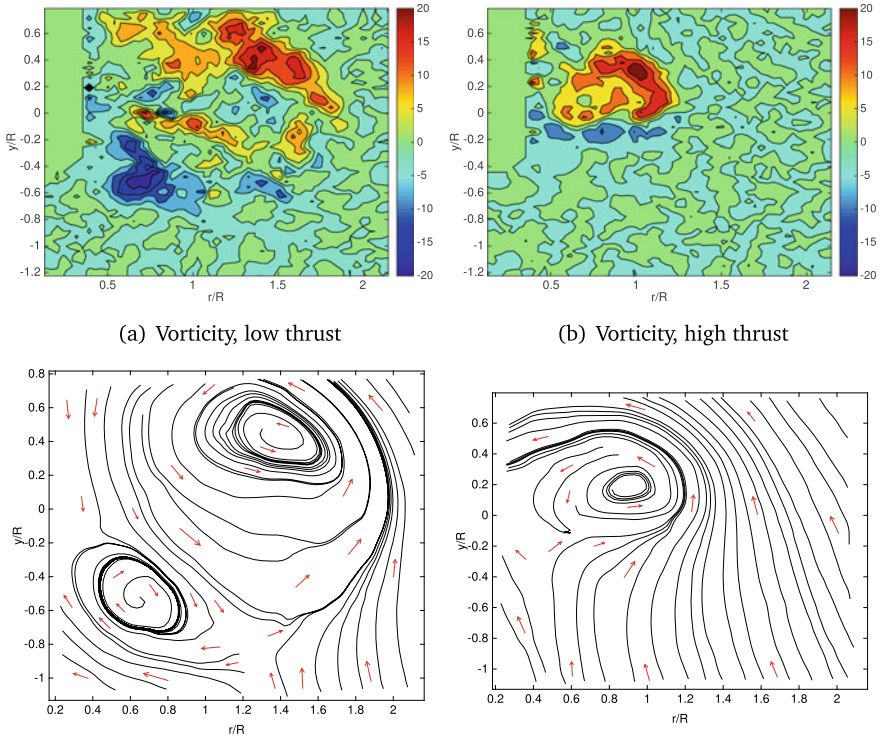

(a) Vorticity, low thrust

(b) Vorticity, high thrust

(c) Streamlines, low thrust

(d) Streamlines, high thrust

Fig. 2.20 PIV of vortex ring state of a rotor in off-axis descent, vorticity and streamlines in symmetry plane (Ö Savaş, University of California at Berkeley [18])

References

1. Goldstein RJ (ed) (1996) Fluid mechanics measurements, 3nd ed. Taylor & Francis. https://doi.org/10.1201/9780203755723
2. Barlow JB, Rae WH, Pope A (1999) Low-speed wind tunnel testing. Wiley-Interscience
3. Bagai A, Leishman JG (1993) Flow visualization of compressible vortex structures using density gradient techniques. Exper Fluids 15:431–442. https://doi.org/10.1007/BF00191786
4. Leishman GJ, Bhagwat MJ, Ananthan S (2004) The vortex ring state as a spatially and temporally developing wake instability. J Am Helicopter Soc 49(2):160–175
5. Raffel M (2015) Background-oriented Schlieren techniques. Exper Fluids 56. https://doi.org/10.1007/s00348-015-1927-5
6. Kindler K, Goldhahn E, Leopold F, Raffel M (2007) Recent developments in background oriented Schlieren methods for rotor blade tip vortex measurements. Exper Fluids 43:233–240. https://doi.org/10.1007/s00348-007-0328-9
7. Shaw-Ward S, Titchmarsh A, Birch DM (2015) Calibration and use of n-hole velocity probes. AIAA J 53. https://doi.org/10.2514/1.J053130
8. Emrich RJ (ed) (1981) Methods of experimental physics, vol 18. Academic Press, Fluid Dynamics, Parts A and B

9. Raffel M, Willert CE, Scarano F, Kahler C, Wereley ST, Kompenhans J (2018) Particle image velocimetry. A Practical Guide Springer. https://doi.org/10.1007/978-3-319-68852-7
10. Prasad AK (2000) Stereoscopic particle image velocimetry. Exper Fluids 29:103–116. https://doi.org/10.1007/s003480000143
11. Albrecht HE, Borys M, Damaschke N, Tropea C (2003) Laser doppler and phase doppler measurement techniques. Springer
12. Zagaglia D, Zanotti A, Gibertini G (2018) Analysis of the loads acting on the rotor of a helicopter model close to an obstacle in moderate windy conditions. Aerospace Sci Technol 78:580–592. https://doi.org/10.1016/j.ast.2018.05.019
13. Prince SA, Green RB, Coton FN, Wang Y (2019) The effect of steady and pulsed air jet vortex generator blowing on an airfoil section model undergoing sinusoidal pitching. J Am Helicopter Soc 64:032004. https://doi.org/10.4050/JAHS.64.032004
14. Zagaglia D, Giuni M, and Green RB (2018) Investigation of the rotor-obstacle aerodynamic interaction in hovering flight. J Am Helicopter Soc 63:032007–1– 032007–12. https://doi.org/10.4050/JAHS.63.032007
15. Visingardi A, De Gregorio F, Schwarz T, Schmid M, Bakker R, Voutsinas S, Gallas Q, Boissard R, Gibertini G, Zagaglia D, Barakos G, Green R, Chirico G, and Giuni M (2017) Forces on obstacles in rotor wake—A GARTEUR action group. 43rd European Rotorcraft Forum, 12th-15th September
16. Pickles D, Green RB, Giuni M (2018) Rotor wake interactions with an obstacle on the ground. Aeronaut J 122(1251):798–820. https://doi.org/10.1017/aer.2018.7
17. Nathan ND, Green RB (2012) The flow around a model helicopter main rotor in ground effect. Exp Fluids 52(1):151–166. https://doi.org/10.1007/s00348-011-1212-1
18. Savaş Ö, Green RB, and Caradonna FX (2009) Coupled thrust and vorticity dynamics during vortex ring state. J Am Helicopter Soc 54:022001–1–0022001–10, 2009. https://doi.org/10.4050/JAHS.54.022001

Richard Green is at the School of Engineering, Glasgow University, where he specialises in wind tunnel testing and instrumentation, a wide array of aerodynamic flows, particularly for rotor systems.